

# Bond behavior between steel and Glass Fiber Reinforced Polymer (GFRP) bars and ultra high performance concrete reinforced by Multi-Walled Carbon Nanotube (MWCNT)

Bitra Hosseinian Ahangarnazhad<sup>\*1</sup>, Masoud Pourbaba<sup>2</sup> and Amir Afkar<sup>3</sup>

<sup>1</sup>Department of Civil Engineering, University of Tabriz, Tabriz, Iran

<sup>2</sup>Department of Civil Engineering, Maragheh Branch, Islamic Azad University, Maragheh, Iran

<sup>3</sup>Research Center of Technology and Engineering, Standard Research Institute, Karaj, Iran

(Received July 30, 2019, Revised February 28, 2020, Accepted March 5, 2020)

**Abstract.** In this paper, the influence of adding multi-walled carbon nanotube (MWCNT) on the pull behavior of steel and GFRP bars in ultra-high-performance concrete (UHPC) was examined experimentally and numerically. For numerical analysis, 3D nonlinear finite element modeling (FEM) with the help of ABAQUS software was used. Mechanical properties of the specimens, including Young's modulus, tensile strength and compressive strength, were extracted from the experimental results of the tests performed on standard cube specimens and for different values of weight percent of MWCNTs. In order to consider more realistic assumptions, the bond between concrete and bar was simulated using adhesive surfaces and Cohesive Zone Model (CZM), whose parameters were obtained by calibrating the results of the finite element model with the experimental results of pullout tests. The accuracy of the results of the finite element model was proved with conducting the pullout experimental test which showed high accuracy of the proposed model. Then, the effect of different parameters such as the material of bar, the diameter of the bar, as well as the weight percent of MWCNT on the bond behavior of bar and UHPC were studied. The results suggest that modifying UHPC with MWCNT improves bond strength between concrete and bar. In MWCNT per 0.01 and 0.3 wt% of MWCNT, the maximum pullout strength of steel bar with a diameter of 16 mm increased by 52.5% and 58.7% compared to the control specimen (UHPC without nanoparticle). Also, this increase in GFRP bars with a diameter of 16 mm was 34.3% and 45%.

**Keywords:** ultra-high-performance concrete; MWCNT; bonding behavior; pullout test; GFRP bars

## 1. Introduction

Ultra-High Performance Concrete (UHPC), also known as reactive powder concrete, is a relatively modern composite material formulated by combining water, Portland cement, quartz flour, silica fume, high-range water reducer, fine silica sand, and steel or other type fibers. Compared with normal concrete, UHPC is known for its high ductility, high strength and high durability. Therefore, UHPC is a topic of interest in recent years for civil engineers and scientists. Great potential application of UHPC has driven increasingly more investments and research into this industry.

In recent investigations, taken advantage and benefit of the nanotechnology, the novel UHPC material with nanoparticle addition was established. Recently, development of nanotechnology has attracted great scientific attention. Due to ultra-fine size of the nanoparticle, addition of nanoparticles results in significantly enhanced mechanical properties of the material without change of the material composition. As a consequence, engineers and researchers are exploring

feasibility of re-engineering many existing materials like concrete by adding nanoparticles into the UHPC material to get new and novel material which has unprecedented performance. Lim *et al.* (2018) investigated the effects of waste ceramic powder and Al<sub>2</sub>O<sub>3</sub>-SiO<sub>2</sub> nanoparticles on both the mechanical and microstructural properties of mortar. Performance of Nano-SiO<sub>2</sub> and Nano-ZnO<sub>2</sub> on compressive strength and microstructure Characteristics of cement mortar and influence of functionalized multi-walled carbon nanotube (MWCNT) on microstructure and mechanical properties of cement paste is investigated by Mousavi and Bahari (2019).

The application of nanoparticles in concrete is one of the options for improving its mechanical properties. Nanoparticles such as nano-Fe<sub>2</sub>O<sub>3</sub>, nano-SiO<sub>2</sub>, nano-TiO<sub>2</sub>, nano-Al<sub>2</sub>O<sub>3</sub>, nano-clay, nano-ZnO<sub>2</sub>, carbon nanotubes (Shoushtari *et al.* 2013, Azim *et al.* 2016), and carbon nanofibers can be used in cementitious materials (Unsal *et al.*, 2017, Janković *et al.* 2019). The brittle nature and fragility of reinforced or UHPC have acted as driving force of the studies to improve the properties of these concretes, and reinforcing the concrete with carbon nanotubes is adopted as a solution. Mechanical properties, slenderness, low specific gravity and corrosion resistance have turned carbon nanotubes into useful materials for reinforcing new building materials. Given that carbon nanotubes have a high length to diameter ratio, they will need more energy to release the

\*Corresponding author, Professor  
E-mail: b.hosseinian.a@gmail.com

cracks around them compared to other fibers (Rezaee and Maleki 2015). Also, their smaller diameter allows more distribution in shorter distances across the concrete. As a result, they are expected to interact with concrete differently than other types of fibers and have more ability to increase the resistance and inhibit the release of cracking. Therefore, reinforcing the concrete with carbon nanotubes, in case it inhibits the formation of larger cracks, can lead to the production of tougher concrete. The results of the studies show that the use of carbon nanotubes significantly improves the performance of conventional concrete, reinforced concrete and UHPC. Kowald *et al.* (2008) studied the effect of carbon nanotubes on micromechanical characteristics of high performance concrete. The results suggest that the use of carbon nanotubes affects the ratios of hydration products. In order to achieve high mechanical characteristics, the dispersion of carbon nanotubes and the linkage between carbon nanotubes and concrete should be optimized. In concrete materials, the use of MWCNT increases compressive strength of the concrete by 30% and 6%, respectively, compared to single-walled carbon nanotubes. Wu *et al.* (2018) empirically investigated the effect of using CaCO<sub>3</sub> nanoparticles on mechanical properties as well as fiber adhesion in UHPC. Their study results showed that the use of 3.2 wt% of CaCO<sub>3</sub> nanoparticles has the best effect on the bond between fibers and concrete and creates the highest compressive strength. The results of Wu *et al.* (2017) also showed that the use of 1 wt% SiO<sub>2</sub> nanoparticle increases fiber bond strength and pullout energy about 35% and 70%, respectively. Norhasri *et al.* (2017) in their review paper examined the impact of using nanomaterial's in UHPC. Their results showed that the use of nanomaterials such as carbon nanotubes with sizes less than 500 nm has the greatest effect on improving the mechanical properties of these types of concretes. Liu *et al.* (2012) added nano-CaCO<sub>3</sub> into the cement paste and the experimental results presented that nano-CaCO<sub>3</sub> particles had no influence on water requirement of normal consistency of the cement mortar. However, with the increase of the nano-CaCO<sub>3</sub> content, its flow ability reduced and setting time of fresh cement paste was decreased. Compressive strength as well as flexural strength improved with the addition of the nano-CaCO<sub>3</sub> at the age of 7 days and 28 days. Mosaberpanah *et al.* (2019) investigated the effect of waste glass powder and nano-silica on rheological, shrinkage, and mechanical properties of UHPC using experimentally and response surface methodology. Liu *et al.* (2020) experimentally investigated the effect of nano-CaCO<sub>3</sub> with different contents (i.e., 0, 1, 2, 3, 4 wt.%) on the mechanical properties including the tensile and compressive strength of the UHPC. The results show that the combination of the nano-CaCO<sub>3</sub> improved the mechanical properties of UHPC, and the optimal nano-CaCO<sub>3</sub> amount to enhance the tensile and compressive properties of UHPC was 3%. More specifically, the compressive strength increased by 7.7%, while the tensile strength increased by nearly 40% up to amount of 3 wt.%.

Another method for reinforcing the mechanical properties of UHPC is to use bar. Therefore, bond strength for concrete structures is one of the most important and

critical issues. The forces used in the concrete and the bar are transmitted by adhesion, friction and load bearing capacity (Midhuna *et al.* 2018). The concrete quality and type, bar diameter, loading type, concrete coating, enclosure, geometry and bar positioning play an important role in creating bond strength (Michal and Keuser 2018). Accordingly, the behavior of UHPC modified with bar of various materials such as steel, GFRP, CFRP, etc., is studied using experimental (Chupin *et al.* 2018, Yan *et al.* 2017), analytical (Bhargava *et al.* 2007, Zhang *et al.* 2017) and numerical (Ozbolt *et al.* 2014, Yoo *et al.* 2017) methods. The main mechanisms in the expansion of bonding are bar-concrete interaction, mechanical interaction between dented or transformed surface of the reinforcing bar and the concrete. Bond resistance of reinforcing bars placed in concrete depends on chemical bonding, frictional stability and shear bonding. Vilanova *et al.* (2015) examined the bonding function of GFRP under sustained loads during the pullout experiment. They tested 12 specimens with 35 and 50 MPa of strength against pullout for 90 and 120-day periods with development lengths of 5 and 10 times of the bar diameter and two reinforcement materials, i.e., GFRP and steel. They concluded that uneven redistribution of tensions may reduce the strength of GFRP bar compared to steel bar. Hung *et al.* (2019) examined the cracking and stiffening behavior of UHPC reinforced with steel bars. Meng and Khayat (2016) simulated the behavior of bending members made of fiber UHPC reinforced with steel bars and glass fibers and verified their results with laboratory results. Using pullout test, Zong-cai *et al.* (2014) also examined the characteristics of the slip bond between high strength bar and UHPC. Some researchers (Lu *et al.* 2018) conducted a direct pullout bond test on specimens to examine the bond strength of concrete, while other researchers (Kâzım 2014) used beam specimens. The results of the studies (Le *et al.* 2018, Ziaei-Nia *et al.* 2018) suggest that UHPC have a higher bond strength than conventional concrete. Pullout behavior of steel fibers with different shapes from UHPC prepared with granite powder under different curing conditions investigated by Zhang *et al.* (2019). Madanipour *et al.* (2016) performed a very large series of pull-out experimental tests on a relatively long bonded lengths in order to identify the development length of a range of reinforcement in the UHPC. The parameters examined include embedded length, casting orientation, cover, bar diameter, compressive strength and bar type. The steel bars investigated included both Grade-60 (414MPa) and Grade-120 (827MPa) reinforcing steel bars, some of which had epoxy coatings. The results show that the higher strength reinforcing bars were important as this prevented the yielding of a significant number of bars for the longer bonded lengths. Also, the relationship between the bond strength and the bonded length for reinforcing bar embedded in UHPC is nearly linear, indicating that UHPC exhibits enhanced performance as compared to conventional high strength concrete. For bars with larger diameter, the bond strength decreases.

A literature review on studying the rebar continuity reinforcement with reinforced concrete shows that the elongation of steel bars and GFRP in modified reinforced

concrete with carbon nanotubes has not been discussed. Accordingly, in the present study, by performing laboratory tests accordance with ACI 440 Committee (2006) and simulation of finite element, the effect of effective parameters on the adhesion of reinforced concrete reinforced with carbon nanotubes has been investigated. For this purpose, firstly, compressive strength, tensile strength and continuity resistance with 28-day processing time and the changes in the amount of nanoscale materials are obtained and then, using a nonlinear finite element model, the adhesive behavior of rebar and reinforced concrete is determined for the cross-sectional dimensions and diameters of the bars. Finally, the numerical modeling results are compared with the results of the extraction test performed on the two samples and the accuracy of the results of the finite element method is examined.

## 2. Experiment procedure

In order to make feasible the comparison between the results, all UHPC used for the purposes of the study had the same water-to-cement ratio. Also, steel grade 500C and GFRP bars with a diameter of 12 and 16 mm (Fig. 1) and with mechanical characteristics listed in Table 1 were used. The materials consisting UHPC include Portland cement, micro silica, quartz powder, silica sand, super lubricant and water. One of the most important materials existing in the composition of UHPC is quartz powder. The mean diameter of its particles is 5.51 mm. Quartz powder is a hard material that improves the specifications of the concrete matrix. The size of the used silica sand particles was in a range of 19.5 to 5.8 mm. Two benefits of silica sand, among the others, are high hardness and ease of access. Cement type 2 was used in producing the specimens. Some physical and chemical characteristics of the cement and micro silica are listed in Table 2. MWCNTs containing carboxylic acid (COOH) groups with a purity percentage greater than 95%, produced by chemical vapor deposition method, were used to improve the properties of UHPC. Figures 2 shows an SEM image of carbon nanotubes generated by transmitted electron microscope (TEM) and Table 3 shows some of their main characteristics.

The nanoparticle were dispersed in a fraction of the mixing water using two types of surfactants. A polyacrylic acid, which is a high molecular weight polyelectrolyte that can be physically adsorbed on the surface of MWCNTs Peyvandi *et al.* (2013), was used to disperse the MWCNTs in the mixing water. The NaDDBS and, SDS, which are surfactants, were incorporated to enhance dispersion. Then, stirring and ultra-sonification were applied using a 800W, cup-horn high intensity ultrasonic processor to ensure greater level of dispersion.

Based on an extensive investigation with measurements of flow characteristics and flexural strength, the following protocol for the dispersion of the nanomaterials was selected Konsta-Gdoutos *et al.* (2010): (1) the MWCNTs, NaDDBS and SDS surfactants and polyacrylic acid were added with a mass ratio of 1:3:4:0.1 in 800-ml water; (2) ultra-sonification was performed for 60 min. In every 70s,

the ultra-sonification was paused for 20s to prevent overheating of the suspensions; (3) stirring was sustained for 3 h before using the dispersed solution in UHPC. Then, a mortar mixer was used to mix this suspension (or water for the cement-based composites without MWCNTs), cement and other parts for about 3 min. Finally, a defoamer was added into the mixture and mixed for another 3 min.

In order to extract the mechanical properties used in finite element analysis, eight different mixtures of concrete were used. Eight different weight percent of MWCNTs, including 0wt%, 0.01wt%, 0.02wt%, 0.03wt%, 0.05wt%, 0.1wt%, 0.2wt% and 0.3wt% were added to the cement mixture. The mix design of various mixtures of concrete prepared with these concentrations of MWCNTs are presented in Table 4, which are shown with U0.00, U0.01, U0.02, U0.03, U0.05, U0.1, U0.2 and U0.3, respectively. In order to determine the tensile and compressive strength of various samples, cube-shaped (60×60×60mm) were used, respectively. Accordingly, Table 5 represents the compressive strength, tensile strength and elasticity modulus of specimens, which were experimentally determined. It should be noted that in order to extract mechanical characteristics of the experiments, each experiment was repeated three times.

The ACI 440 Committee has developed some test methods for concrete structures reinforcing by fiber reinforced polymer bars, including bar pullout test. The main purpose of pullout test is to obtain the bond strength between concrete and bar. The main variable is the mechanical properties and type of the bar, as well as the volume fraction of MWCNTs. A review of the ASTM 944-99 standard demonstrations that the pullout test guideline for metal bars highly resembles the ACI 440 standard. Consequently, the steps of preparing and testing steel bars were the same of that in polymer bars. Other conditions of testing are similar to those suggested in Veljkovic *et al.* (2017), and the pullout test was carried out after processing the specimens for 28 days in water.



Fig. 1 The surface of the used steel (a) and GFRP (b) bars

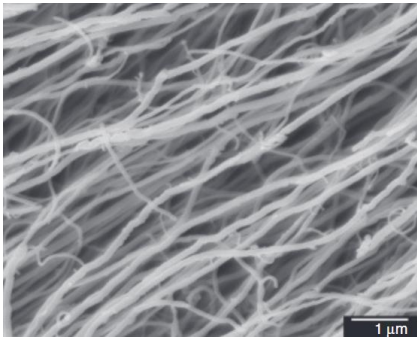


Fig. 2 SEM image of MWCNTs

Table 1 Mechanical properties of the used bars

	Nominal diameter (mm)	Tensile strength (MPa)	Young Modulus (GPa)
GFRP bar	12, 16	896	46
Steel bar grade 500C	12, 16	500	210

Table 2 Chemical characteristics of Portland cement and micro silica powder

Constituent	Silica fume (mass %)	OPC (mass %)
SiO <sub>2</sub>	93.0	21.9
Al <sub>2</sub> O <sub>3</sub>	0.4	4.9
Fe <sub>2</sub> O <sub>3</sub>	0.5	3.6
CaO	0.8	62.4
MgO	0.4	2.0
K <sub>2</sub> O	0.8	0.5
LOI	1.5	1.78
SO <sub>3</sub>	-	2.1
Na <sub>2</sub> O	-	0.4
Sum	97.4	99.5

Table 3 Specifications of MWCNTs

Property	Unit	Value
CNT type	-	Bundle
Bundle length	μm	10-55
Outer diameter	nm	8-14
Bundle diameter	nm	2-18
Bundle density	g/ml	0.02-0.04
Purity	%	95
Crystallinity	-	CVD

In accordance with ACI 440 Committee (2006) the UHPC specimens used in this study had a length and width of 200mm and their geometric characteristics is presented in

Fig. 3; where  $l$  represents the free length of the bar and  $d_f$  represents the diameter of the bar. According to the ACI 440 committee (2006), the embedded length between the bar and concrete was considered  $l=5 d_f$ . Along the remaining part of the bar, an aluminum pipe was inserted to prevent bond between bar and concrete. Aluminum pipe prevented forming of the bond between UHPC and the bar along the bond-free length. Also, Fig. 4 shows the laboratory specimens prepared to test the tensile and determine the compressive strength of the specimens. Figure 5 shows the configuration of pullout tests. As shown in Fig. 4, the concrete specimens were placed on a steel box and the free end of the bar was fixed by the jaws of the device. In order to carry out empirical tests, a Universal Testing Machine with a maximum load of 20kN was used. The displacement-controlled loading was supposed to capture the behavior of the bond in the load decreasing phase. The cross head displacement rate was fixed to 0.5 mm/min and the tests was stopped when bond stress was lower than 10% of its maximum value. In order to record the displacement, the linear variable differential transformer (LVDT) displacement sensor attached on the top of the UHPC specimen was used and the relative displacement between the steel frame and the specimen was measured. The difference between two relative displacements represents the slip between bar and the concrete.

Table 4 The mix design of examined specimens

Concrete ID	Binder		MWCNTs	Water	Admixture (SP)
	Cement	Silica fume			
U0.00	850	150	0.00	200	0.5
U0.01	850	150	0.01	200	0.7
U0.02	850	150	0.02	200	1.1
U0.03	850	150	0.03	200	1.5
U0.05	850	150	0.05	200	2.0
U0.1	850	150	0.10	200	2.5
U0.2	850	150	0.20	200	5.5
U0.3	850	150	0.30	200	7.8

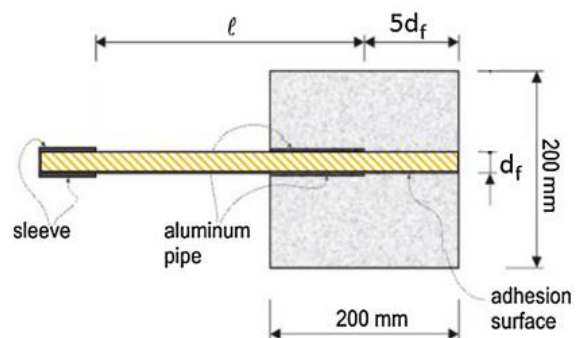


Fig. 3 Geometric specifications of specimens examined



Fig. 4 Laboratory specimens prepared for pullout testing and compressive strength determination



Fig. 5 Pull-out experimental set-up

Table 5 Overview of performed tests and specimen ID

Concrete ID	Bar material	Bar diameter (mm)	Specimen ID
U0.00	GFRP		C12(16)U0.00
	Steel		S12(16)U0.00
U0.01	GFRP		C12(16)U0.01-(FEM & Exp)
	Steel		S12(16)U0.01-(FEM & Exp)
U0.02	GFRP		C12(16)U0.02
	Steel		S12(16)U0.02
U0.03	GFRP	12, 16	C12(16)U0.03
	Steel		S12(16)U0.03
U0.05	GFRP		C12(16)U0.05
	Steel		S12(16)U0.05
U0.1	GFRP		C12(16)U0.1
	Steel		S12(16)U0.1
U0.2	GFRP		C12(16)U0.2
	Steel		S12(16)U0.2
U0.3	GFRP		C12(16)U0.3
	Steel		S12(16)U0.3

The samples used for pullout tests were named as follows: the first letter indicates the type of bar used (S = Steel and C = GFRP), which follows with bar diameter (12 mm and 16 mm). Next, the material of the concrete (U0.0-U0.3, as given in Table 4) and then the manner of extracting the results (Exp or FEM) are presented. For example, C12U0.1 represents the use of GFRP bar with a diameter of 12mm in concrete U0.1. Table 5 represents the various combinations of the above parameters used in the analysis. It should be noted that the results of the finite element model were verified by empirical extraction experiments for specimens C12U0.01 and S12U0.01.

## 2.1 Numerical modelling and FEM

In this study, to extend the experimental results to the finite element modeling, pullout test was used regarding the bar. The 3D pullout test was simulated using ABAQUS software. In 3D models, cohesive element is used to define the interaction and bond between bars and concrete and in order to validate numerical models, the initial results of the finite element were compared with the experimental results and the finite element models were calibrated.

In 3D simulation, given that all force is exerted into a node, the spring elements cannot be used. Accordingly, in the present study, cohesive elements were used to solve this problem. In the present paper, the analysis of bar separation from concrete was simulated using cohesive surface and cohesive zone model (CZM). Mechanical behavior of the contact surface modeled as a cylinder around the bar is simulated using the stress-separation law and based on exponential cohesive zone model. In this model, the behavior of which is shown in Fig. 6, in the absence of any failure, the behavior of the contact surface is assumed linear and this behavior will terminate with the occurrence of the failure. The criterion of failure initiation in proposed method is based on the maximum stress criterion and is expressed as follows

$$\left(\frac{\tau_n}{\tau_n^{\max}}\right)^2 + \left(\frac{\tau_s}{\tau_s^{\max}}\right)^2 + \left(\frac{\tau_t}{\tau_t^{\max}}\right)^2 = 1 \quad (1)$$

where,  $\tau_n$ ,  $\tau_s$  and  $\tau_t$  are normal, tangential and shear components of the stress applied to the contact surface, respectively. The fracture energy,  $G_b$ , is another parameter which is effective in determining the behavior of the contact surface, and its value is equal to the area below the curve of Fig. 6. The failure model of the contact surface assumes that the energy consumed in the collapse of the contact surface is independent of the loading path, and the value of the fracture energy is expressed as

$$G_b = \frac{1}{2} t_b \Delta \delta \quad (2)$$

where,  $t_b$  is the strength of the sticky region and  $\delta$  is the displacement along this area. In numerical modeling, the tensile fracture energy of the concrete,  $G_b$ , according to CEB-FIP regulations (1999), was used as follows

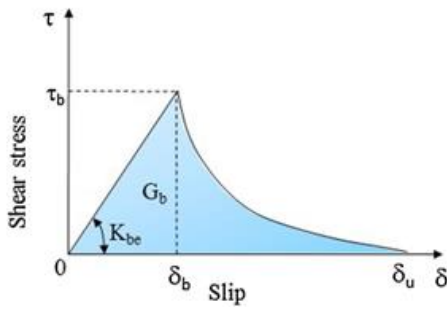


Fig. 6 The standard stress-separation behavior

$$G_b = G_{b0} \left( \frac{f_c'}{10} \right)^{0.7} \quad (3)$$

where,  $G_{b0}$  is the base fracture energy that its value is selected 0.03N/mm based on calibration results.

Mechanical properties of the UHPC specimens modified with MWCNTs were determined experimentally and the properties of the adhesive elements were selected after calibration based on the experimental results, so that the results of the force-displacement of the bars be similar to that of the experimental results.

Due to symmetric geometry of the model and decline analysis time, the quarter model was used. The models were meshed using 20-node 3D cubic elements and a nonlinear quasi-static method was used to analyze the problem. In the models under investigation, according to the experimental model, the lower surface of the concrete specimens was fully bounded and the maximum displacement applied to the upper part of the bar will be 2 mm. Given that the areas around the bar are more sensitive, so smaller elements were used in these areas. Fig. 7 shows the finite element model along with the boundary and loading conditions.

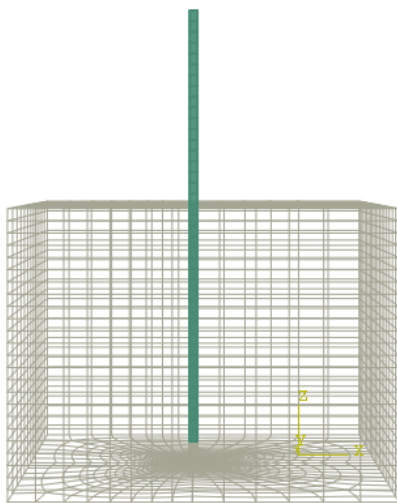


Fig. 7 Finite element model of the pullout test along with boundary and loading conditions

### 3. Results and discussion

By performing bar pullout tests, as well as the finite element results, we can obtain the maximum amount of the force between steel bars with different diameters and UHPC. Also, using the following equation, we can determine the mean bond stress of steel bars and UHPC for each specimen

$$\tau = \frac{F}{(5.\phi).(\pi.\phi)} \quad (4)$$

where,  $\tau$  is the bond stress,  $F$  is the tensile force measured at the moment of fracture and  $\phi$  is bar diameter. Assuming the shear stress ( $\tau$ ) constant along the contact surface of the bar and concrete, the shear stress curves in terms of bar displacement will be examined in order to reveal the effect of bar diameter and shape, as well as the volume percent of used MWCNTs, on the bond of the bar and concrete.

#### 3.1 The effects of MWCNTS on the mechanical properties of UHPC

First, the effect of the weight percent of the nanotubes on the mechanical properties of the UHPC will be examined. These results that obtain from empirical tests of 28-day specimens, will be used as inputs for the software and finite element analyses. Table 6 shows the mechanical properties including compressive strength, tensile strength and elasticity modulus of the UHPC specimens with the mixes represented in Table 4. As can be seen, the weight percent of the used MWCNTs has a significant effect on the mechanical properties of UHPC, and mechanical properties such as tensile strength and compressive strength of these materials are initially increasing and then decreasing by increasing the weight percent of MWCNTs. Therefore, there is a certain amount of weight percent for which the most mechanical properties are achievable. For example, in the used mix design, MWCNTs with 0.01 wt%, have the most effective impact on the tensile and compressive strength of the UHPC. According to Fig. 6, in which the percentage increase in compressive strength, tensile strength and elastic modulus is shown compared to the base specimen (U0.00), it can be seen that adding 0.01 wt% of MWCNTs to the UHPC increases the compressive strength, tensile strength and elastic modulus 18.8%, 22.6% and 14.3%, respectively. This amount of MWCNTs reduces the porosity of UHPC and, as a result, creates a more compact and continuous concrete nanocomposite. In this case, the use of MWCNTs in the concrete matrix, by creating more contact surfaces and consequently more force transfer surfaces, results in better bond between nanotube with the concrete matrix around it, and hence the nanotubes are considered the main load bearing component.

The other result that can be observed is that by increasing the percentage of MWCNTs, these materials weaken the tensile and compressive strength of UHPC. The lower tensile and compressive strength of UHPC in relation to the specimen containing more than 0.03 wt% MWCNTs compared to the one containing 0.02 wt% of MWCNTs can

be attributed to the reduction in the bond of carbon nanotubes with concrete due to the formation of a non-continuous network in the context and also formation of defects and particles agglomeration and cracking of carbon nanotubes phenomena in high percentages of MWCNTs.

According to Table 6, it is evident that the effect of adding MWCNTs in a certain weight percentage is greater on the tensile strength than the flexural strength of the specimen. It should also be noted that accumulation of MWCNTs and agglomeration phenomena in the specimen containing more than 0.1 wt% of MWCNTs, due to the formation of weak regions, causes a sharp decrease in the shear strength of the UHPC; so that, the tensile strength of the specimen containing 0.3 wt% of MWCNTs is about 23% less than the base specimen. To add high amounts of MWCNTs due to poor distribution within the concrete results in the formation of agglomerates consisting of MWCNTs. Agglomerates act as stress concentration areas and reduce the force required for crack propagation, and consequently result in concrete fracture. Agglomerates also cause cracks converge, and also act as the primary regions of cracking. Consequently, the effect of these regions on tensile strength reduction is much greater than the compressive strength loss.

Moreover, the Young's modulus of elasticity in flexure represented by the initial lobe of the force-displacement curve was computed for each UHPC mix and the variation of this modulus is shown in Table. 6. Another finding of Table. 6 is that although unlike the tensile and compressive strengths, elasticity modulus increase with the increase in the dosage of MWCNTs, but for the amounts more than 0.05wt% of MWCNTs, the increasing rate of elastic modulus will be decreasing. The modulus of elasticity of UHPC increased by 5% with adding 0.01% MWCNTs, and increased by 22% with 0.3% MWCNTs. Presence of MWCNTs in the context limits the movement of concrete components, which increases the stiffness of the concrete. Also, due to the high modulus of carbon nanotubes compared to the concrete, the increase in the concrete elasticity modulus is common.

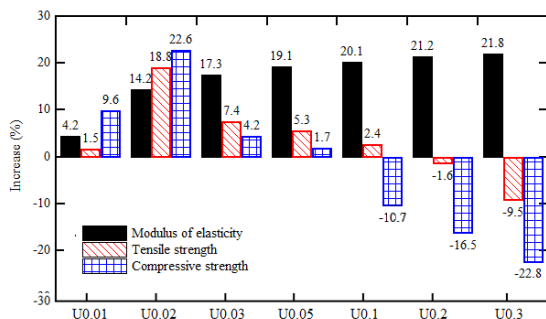


Fig. 8 The percentage of increase in compressive strength, tensile strength and elastic modulus compared to the base specimen (U0.00)

Table 6. Tensile strength, compressive strength and modulus of elasticity of the considered concretes

Concrete ID	Compressive strength (MPa)		Tensile strength (MPa)		Modulus of elasticity (GPa)	
	Average	St. Dev.	Average	St. Dev.	Average	St. Dev.
U0.00	165	-	15.3	-	43.2	-
U0.01	167	0.57	16.5	0.6	45.1	4.21
U0.02	204	0.83	18.6	0.60	50.4	14.28
U0.03	200	0.41	15.8	1.03	52.3	17.39
U0.05	181	0.30	15.3	1.24	53.4	19.10
U0.1	175	0.34	14.2	0.78	54.1	20.11
U0.2	168	0.62	13.7	0.49	54.8	21.16
U0.3	154	0.65	13.2	0.82	55.3	21.88

Reduction in the increasing rate of elastic modulus per addition of more weight percent of MWCNTs probably is due to agglomeration of carbon nanotubes within the context, which reduces their effect on improving the stiffness of the material.

### 3.2 Verification of the finite element model

After developing the initial model of the finite element in accordance with the laboratory test specification, finite element analysis was carried out on the model and the resultant force-displacement curve was investigated. Finally, in order to achieve a realistic result and close to the experimental results, the finite element model was calibrated. The changes were made by considering the specifications of the laboratory specimen and in order to improve and approximate the specifications of force-displacement curve resulted from the finite element to the experimental results. The force-displacement curve for the final model of the finite element of C12U0.01 specimen and the overlap between the two results obtained from laboratory studies and finite element model are shown in Fig. 7.

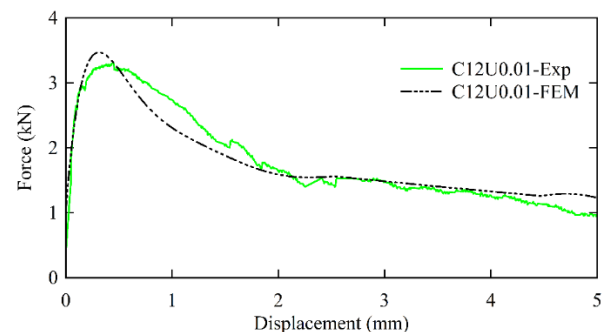


Fig. 9 Comparing the force-displacement curve obtained from finite element model with experimental results of C12U0.01 specimen

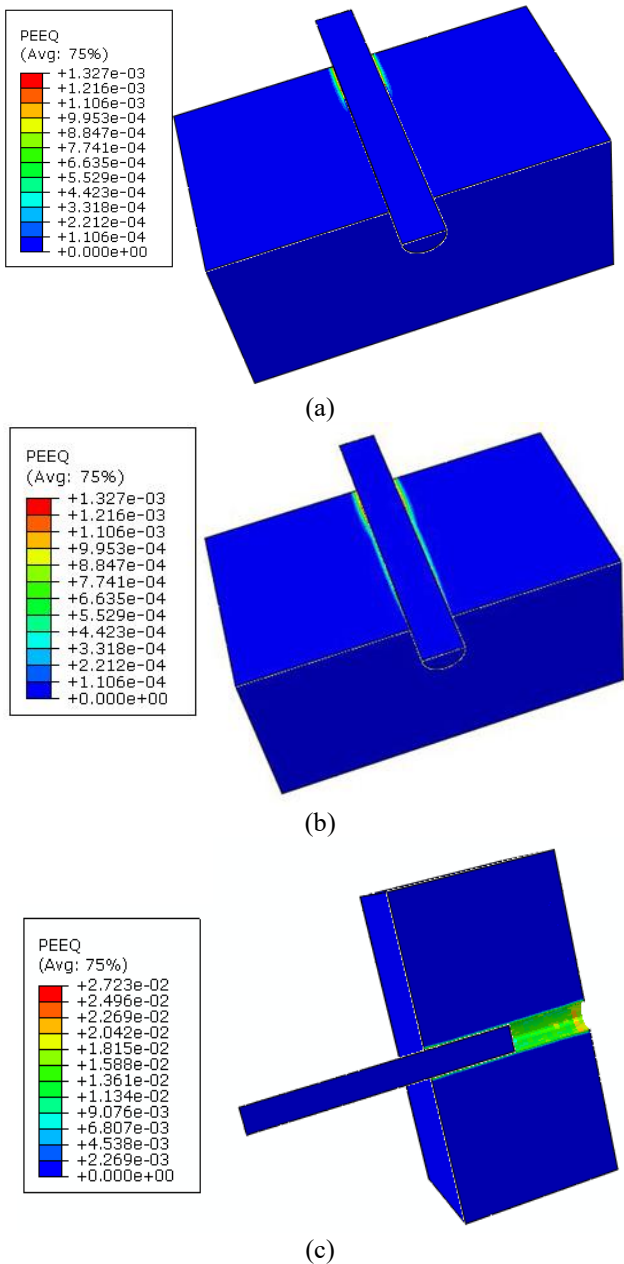


Fig. 10 Distribution of plastic strain for different amounts of force for C12U0.01 specimen; (a) a force of 0.5kN; (b) a force of 2kN; and (c) a force of 3.4kN

As can be seen, there is an optimal overlap both in terms of curvature and the maximum pullout force of the laboratory specimen and the finite element model is established and there is about 3% error in the maximum pullout force in the laboratory specimen compared to the finite element specimen. The origin of some error factors can be finding in the lack of full compliance between the boundary conditions of finite element and experimental models, initial stresses and the effects of initial defects.

### 3.3 The effect of bar materials

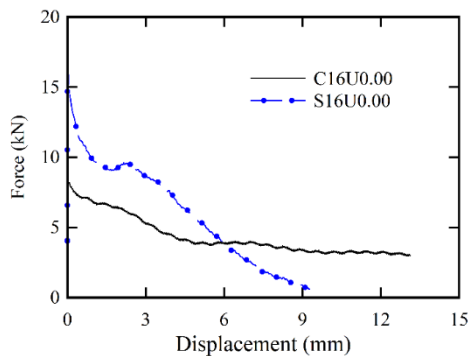
In this section, the advantages and disadvantages of two

different kinds of materials used in bar, i.e., GFRP and steel, on the results of pullout test in UHPC will be examined. To that end, concrete with a mix design of U0.00, with GFRP and steel bars with diameters of 12 mm and 16 mm, will be examined. The force-displacement curves of the specimens are presented in Fig. 9. As it can be seen, due to the high bonding strength of UHPC with steel bars, the maximum force required to pull out 12mm and 16mm steel bars from a 28-day UHPC with a mix design of U0.00 were about 78.8% and 65.9%, respectively, more than that for similar specimen with GFRP bar. Examining the results for different diameters shows that an increase in bar diameter leads to a significant increase in the maximum force required to pullout the bar. Also, due to improvement in chemical bonding between UHPC and GFRP bar, an increase in the diameter of the bar from 12 mm to 16 mm leads to an increase from 3.4 kN to 9.2 kN, and consequently the maximum force required to pullout the bar will increase about 63%. The reason can be explained by a strengthened chemical adhesion mechanism in case of increasing the bars diameter. In addition, it can be seen that the maximum adhesion force between steel bars of 12 mm and 16 mm in diameter and concrete is about 5.4 kN and 14.8 kN, respectively; so, the increase in bar diameter has led to an increase by 75% in maximum pullout force. Given that in the specimens reinforced with GFRP bars, unlike steel bars, there is no indentation on the surface of the bar, so the bar will have no mechanical engagement with the concrete and consequently there will be no static resistance, thus the pullout force for GFRP bars will be lower than that for steel bars.

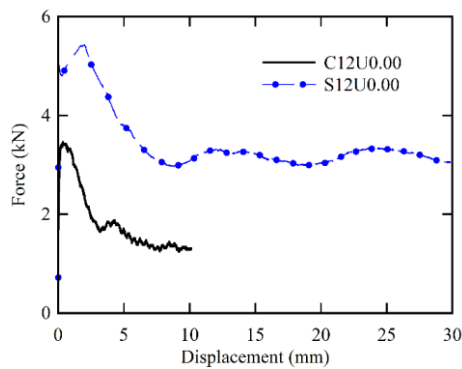
For a closer examination of the interaction between GFRP bar and UHPC, different regions of the force-displacement curve for C12U0.00 specimen are shown in Fig. 10. It can be seen from the figure that at the beginning of loading, the OA section, with the onset of the force, its value increases to reach the bar slipping threshold (point A). By increasing the force as a result of higher shear stresses, the chemical adhesion between the GFRP bar and concrete is weakened and the adhesion force decreases and this phenomenon continues to point B. At this point, the chemical adhesion is completely eliminated and the shear friction adhesion mechanism is a factor affecting the bond between the bar and the concrete. Given that the friction coefficient is relatively constant, therefore, in the BC region, with increase in the amount of displacement, the force required to pullout the bar remains constant.

In GFRP bar, depending on the friction resistance of the bars, the slip occurs outward, and consequently the fracture will be of a sliding type. In steel bars, given that they are indented, in addition to chemical bonding and frictional stability, mechanical fastening between concrete and bar indentations can increase the bond strength. Among the adhesion mechanisms, shear adhesion of indented bar to concrete is of particular importance because it creates the greatest stress in bonding. In this bonding mechanism, the force transmission occurs through the involvement of bar indentations and concrete keys between them. Fig. 11 shows how GFRP and steel bars have separated after empirical tests. According to the results, when the

maximum bond stress obtains, the load bearing mechanism eliminates and the residual bond strength essentially becomes dependent on the frictional resistance. After conducting the tests and examining the fracture behavior of the specimens, it became revealed that the steel bars in these experiments were removed through cracking the concrete and creating vertical cracks, but the polymer bars, due to weak bond, were removed sliding. None of the steel bars reached the yield stress, and also regarding polymer bars, none of them reached the boundary of the bar fibers fall apart.



(a)



(b)

Fig. 11 Force-displacement curves for various specimens of UHPC modified without MWCNTs and steel and GFRP bars

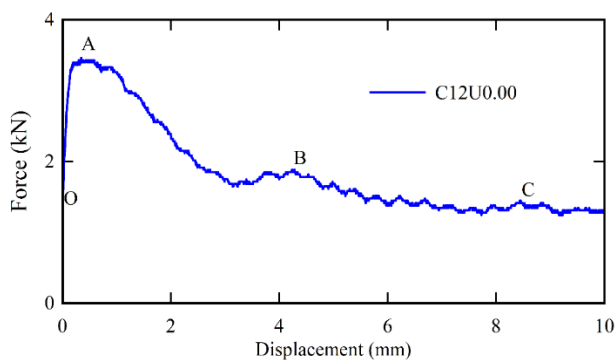


Fig. 12 Slipping mechanism for C12U0.00 specimen



(a)



(b)

Fig. 13 The separation of (a) GFRP and (b) steel bars after experimental tests

### 3.4 The effect of modifying UHPC with MWCNTs

UHPC, due to the use of pozzolan and chemical compounds, is highly resistant with good filling properties. In the present study, MWCNTs is used to increase the filling characteristic and improve mechanical properties of UHPC. As mentioned earlier, given that the effect of modifying the properties of UHPC with MWCNTs on adhesion between bar and concrete has not yet been investigated, then in this section, the results of pullout tests for concrete specimens reinforced with MWCNTs will be discussed. The force-displacement curves for different specimens of UHPC modified with MWCNTs, and steel and GFRP bars are presented in Figs. 12 and 13. According to the results presented in Fig. 12, in the mixing designs of UHPC, with the increase (0.01 and 0.02) in the percentage of MWCNTs (% of cement weight), the maximum pullout force for steel bars with diameter of 16mm will increase

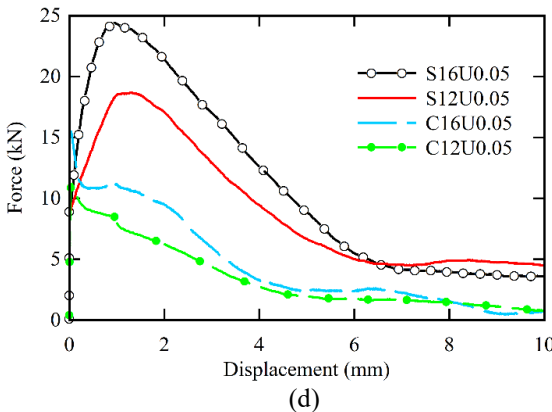
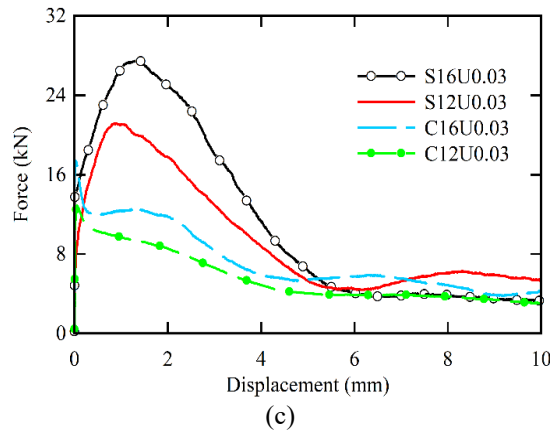
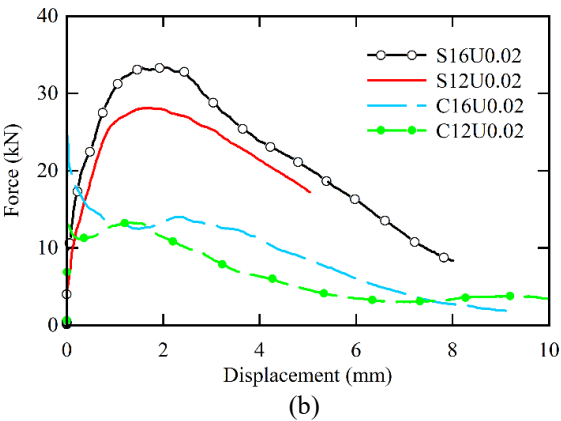
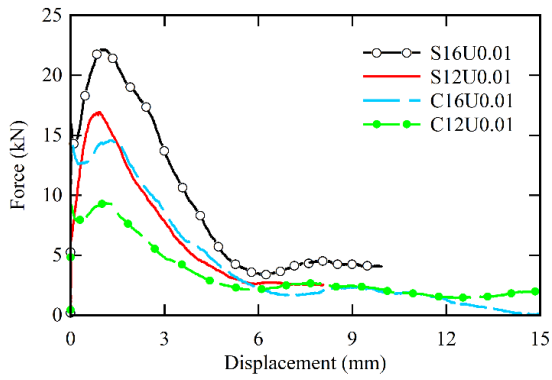


Fig. 14 Force-displacement curves for various specimens of UHPC modified with MWCNTs

52.5 % and 58.7% compared to the control specimen, respectively. Also, according to Fig. 12, this increase for GFRP bars with a diameter of 16mm is 34.2% and 45%. The results show that the use of MWCNTs can significantly improve the bond behavior between bar and UHPC modified with MWCNTs. Improved bond behavior of the bars and UHPC due to addition of MWCNTs can be attributed to the mechanical and chemical mechanisms that improve microstructures and consequently increase the mechanical properties and durability of the concrete.

**5. Conclusions**

In the present study, using empirical tests and finite element model, the bond behavior of GFRP and steel bars with UHPC modified with MWCNTs was examined. After conducting the pullout test on several laboratory specimens, the maximum slip force and slip displacement between the bar and concrete were calculated.

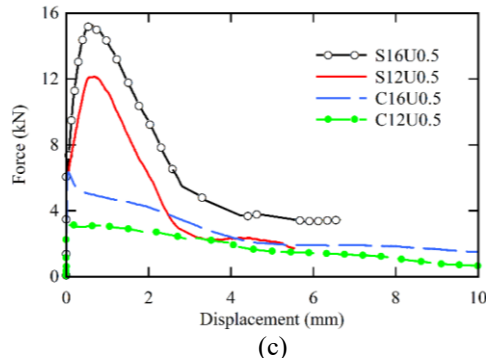
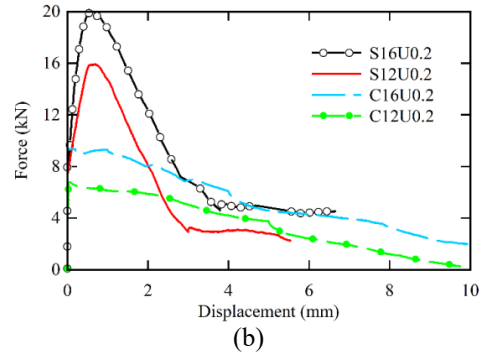
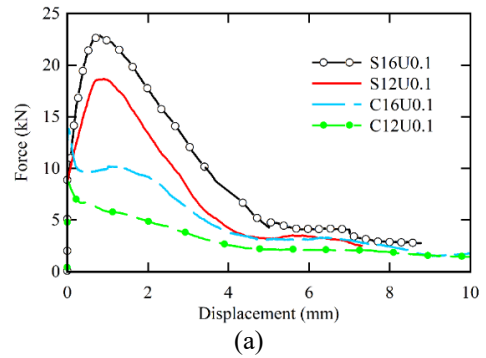


Fig. 15 Force-displacement curves for various specimens of UHPC modified with GFRP bars and nanoparticles

In addition, the effect of factors such as the type and diameter of the bar, along with the volume percent of MWCNTs, on the bond strength were evaluated. The results showed that the steel bars have a better bond strength in compare with polymer bars in different kinds of concrete. The results for the control specimen lacking nanoparticles show that due to more bond between concrete and steel bars, the maximum force required to pullout the bar for steel bars with a diameter of 12 mm and 16 mm is about 78.8% and 65.9% higher than that for similar specimens with CFRP bar. In addition, the use of MWCNTs, due to its high reactivity, increases the maximum bond force between bar and light weight self-compacting concrete. In the mix design of UHPCs an increase (0.01 and 0.02) in wt% of MWCNTs (percentage of cement weight), the maximum force required to pull out a steel bar with 16 mm diameter will increase by 52.5% and 58.7%, in compare with the control specimen. Also, this increase for GFRP bars with a diameter of 16mm will be 34.2% and 45%.

## References

- Azim, R. and Amiri G., (2016), "The effects of near and far fault accelerograms modification on seismic behaviour of concentrated braced steel frames", *J. Res. Sci., Eng. Technol.*, **4**(1), 12-21.
- Bhargava, K., Ghosh, A., Mori, Y. and Ramanujam, S. (2007), "Corrosion-induced bond strength degradation in reinforced concrete—Analytical and empirical models", *Nuclear Eng. Design*, **237**(11), 1140-1157. <https://doi.org/10.1016/j.nucengdes.2007.01.010>.
- Chupin, O., Piau, J.M., Hammoum, F. and Bouron, S. (2018), "Experimental study and modeling of the behavior of partially saturated asphalt concrete under freezing condition", *Constr. Build. Mater.*, **163**, 169-178. <https://doi.org/10.1016/j.conbuildmat.2017.12.070>.
- Committee, A. (2006), "Guide for the Design and Construction of Concrete Reinforced with FRP Bars (ACI 440.1 R-06)", *American Concrete Institute, Detroit, Michigan*.
- Dehestani, M., Asadi, A. and Mousavi, S. (2017), "On discrete element method for rebar-concrete interaction", *Constr. Build. Mater.*, **151**, 220-227. <https://doi.org/10.1016/j.conbuildmat.2017.06.086>.
- Hung, C.C., Lee, H.S. and Chan, S.N. (2019), "Tension-stiffening effect in steel-reinforced UHPC composites: Constitutive model and effects of steel fibers, loading patterns, and rebar sizes", *Compos. Part B: Eng.*, **158**, 269-278. <https://doi.org/10.1016/j.compositesb.2018.09.091>.
- Janković, K., Bojović, D. and Stojanović, M. (2019), *2 - Influence of nanoparticles on the strength of ultra-high performance concrete, in Nanotechnology in Eco-efficient Construction (Second Edition)*, (Eds., F. Pacheco-Torgal, M.V. Diamanti, A. Nazari, C.G. Granqvist, A. Pruna, and S. Amirkhanian), Woodhead Publishing, 13-42.
- Kâzım, T. (2014), "Bond strength of tension lap-splices in full scale self-compacting concrete beams", *Turkish J. Eng. and Environ. Sci.* **32**(6), 377-386.
- Konsta-Gdoutos, M.S., Metaxa, Z.S. and Shah, S.P. (2010), "Highly dispersed carbon nanotube reinforced cement based materials", *Cement Concrete Res.*, **40**(7), 1052-1059. <https://doi.org/10.1016/j.cemconres.2010.02.015>.
- Kowald, T. (2008), *Influence of Carbon Nanotubes on the micromechanical properties of a model system for ultra-high performance concrete*, 2nd International Symposium on Ultra High Performance Concrete, USA.
- Le, A.H., Ekkehard, F., Thai, D.K. and Nguyen, C.V. (2018), "Simplified stress-strain model for circular steel tube confined UHPC and UHPFRC columns", *Steel Compos. Struct.*, **29**(1), 125-138. <https://doi.org/10.12989/scs.2018.29.1.125>.
- Lim, N.H.A.S. (2018), "Microstructure and strength properties of mortar containing waste ceramic nanoparticles", *Arabian J. Sci. Eng.*, **43**(10), 5305-5313.
- Liu, X., Chen, L., Liu, A. and Wang, X. (2012), "Effect of nano-CaCO<sub>3</sub> on properties of cement paste", *Energy Procedia*, **16**, 991-996. <https://doi.org/10.1016/j.egypro.2012.01.158>.
- Liu, X.F. (2020), *Mechanical Properties of Nano-Particle Modified Ultra-High Performance Fiber Reinforced Concrete*. in *ACMSM25*, Singapore: Springer Singapore.
- Lu, Y., Liu, Z., Li, S. and Li, N. (2018), "Bond behavior of steel fibers reinforced self-stressing and self-compacting concrete filled steel tube columns", *Constr. Build. Mater.*, **158**, 894-909. <https://doi.org/10.1016/j.conbuildmat.2017.10.085>.
- Meng, W. and Khayat, K.H. (2016), "Experimental and numerical studies on flexural behavior of ultrahigh-performance concrete panels reinforced with embedded glass fiber-reinforced Polymer grids", *Transportation Research Record*, **2592**(1), 38-44. <https://doi.org/10.3141/2592-05>.
- Midhuna, M.S., Gunneswara, T.D. and Chaitanya Srikrishna, T. (2018), "Mechanical and fracture properties of glass fiber reinforced geopolymer concrete", *Adv. Concrete Constr.*, **6**(1), 29-45. <https://doi.org/10.12989/acc.2018.6.1.029>.
- Michal, M. and Keuser, M. (2018), *Bond Tests Under High Loading Rates*, in *High Tech Concrete: Where Technology and Engineering Meet*, 1453-1461.
- Mosaberpanah, M.A., Eren, O. and Tarassoly, A.R. (2019), "The effect of nano-silica and waste glass powder on mechanical, rheological, and shrinkage properties of UHPC using response surface methodology", *J. Mater. Res. Technol.*, **8**(1), 804-811.
- Mousavi, M.A. and Bahari, A. (2019), "Influence of functionalized MWCNT on microstructure and mechanical properties of cement paste", *Sādhanā*, **44**(5), 103. <https://doi.org/10.1007/s12046-019-1087-z>.
- Norhasri, M.S.M., Hamidah, M.S. and Fadzil, A.M. (2017), "Applications of using nano material in concrete: A review", *Constr. Build. Mater.*, **133**, 91-97. <https://doi.org/10.1016/j.conbuildmat.2016.12.005>.
- Ožbolt, J., Oršanić, F. and Balabanić, G. (2014), "Modeling pull-out resistance of corroded reinforcement in concrete: Coupled three-dimensional finite element model", *Cement Concrete Compos.*, **46**, 41-55. <https://doi.org/10.1016/j.cemconcomp.2013.10.014>.
- Peyvandi, A., Soroushian, P., Abdol, N. and Balachandra, A.M. (2013), "Surface-modified graphite nanomaterials for improved reinforcement efficiency in cementitious paste", *Carbon*, **63**, 175-186. <https://doi.org/10.1016/j.carbon.2013.06.069>.
- Rezaee, M. and Maleki, V.A. (2015), "An analytical solution for vibration analysis of carbon nanotube conveying viscose fluid embedded in visco-elastic medium", *Proceedings of the Institution of Mechanical Engineers, Part C: Journal of Mechanical Engineering Science*, **229**(4), 644-650.
- Shoushtari, A., Sharafi, M. and Sekhavat, S. (2013), "Effect of Solution Annealing Heat Treatment on the Corrosion Resistance and Mechanical Properties of an Austenitic Stainless Steel", *Uct J. Res. Sci., Eng. Technol.*, **1**(4), 17-20.
- Solomos, G. and Berra, M. (2010), "Rebar pullout testing under dynamic Hopkinson bar induced impulsive loading", *Mater. Struct.*, **43**(1-2), 247-260. <https://doi.org/10.1617/s11527-009-9485-z>.
- Unsal, I., Tokgoz, S., Cagatay, I.H. and Dundar, C. (2017), "A study on load-deflection behavior of two-span continuous concrete beams reinforced with GFRP and steel bars", *Struct.*

- Eng. Mech.*, **63**(5), 629-637.  
<https://doi.org/10.12989/sem.2017.63.5.629>.
- Veljkovic, A., Carvelli, V., Haffke, M.M. and Pahn, M. (2017), "Concrete cover effect on the bond of GFRP bar and concrete under static loading", *Compos. Part B: Eng.*, **124**, 40-53.  
<https://doi.org/10.1016/j.compositesb.2017.05.054>.
- Vilanova, I., Baena, M., Torres, L. and Barris, C. (2015), "Experimental study of bond-slip of GFRP bars in concrete under sustained loads", *Compos. Part B: Eng.*, **74**, 42-52.  
<https://doi.org/10.1016/j.compositesb.2015.01.006>.
- Wu, Z., Khayat, K.H. and Shi, C. (2017), "Effect of nano-SiO<sub>2</sub> particles and curing time on development of fiber-matrix bond properties and microstructure of ultra-high strength concrete", *Cement Concrete Res.*, **95**, 247-256.  
<https://doi.org/10.1016/j.cemconres.2017.02.031>.
- Wu, Z., Shi, C. and Khayat, K.H. (2018), "Multi-scale investigation of microstructure, fiber pullout behavior, and mechanical properties of ultra-high performance concrete with nano-CaCO<sub>3</sub> particles", *Cement Concrete Compos.*, **86**, 255-265. <https://doi.org/10.1016/j.cemconcomp.2017.11.014>
- Yan, F. (2017), "Experimental study on bond durability of glass fiber reinforced polymer bars in concrete exposed to harsh environmental agents: freeze-thaw cycles and alkaline-saline solution", *Compos. Part B: Eng.*, **116**, 406-421.  
<https://doi.org/10.1016/j.compositesb.2016.10.083>.
- Yoo, D.Y., Kang, S.T., Banthia, N. and Yoon, Y.S. (2017), "Nonlinear finite element analysis of ultra-high-performance fiber-reinforced concrete beams", *Int. J. Damage Mech.*, **26**(5), 735-757. <https://doi.org/10.1177/1056789515612559>.
- Madanipour, V., Montazeri-Gh, M. and Mahmoodi-k, M. (2016), "Optimization of the component sizing for a plug-in hybrid electric vehicle using a genetic algorithm", *Proceedings of the Institution of Mechanical Engineers, Part D: J. Automobile Eng.*, **230**(5), 692-708.
- Zhang, H., Ji, T. and Lin, X. (2019), "Pullout behavior of steel fibers with different shapes from ultra-high performance concrete (UHPC) prepared with granite powder under different curing conditions", *Constr. Build. Mater.*, **211**, 688-702.  
<https://doi.org/10.1016/j.conbuildmat.2019.03.274>.
- Zhang, X., Ou, J. and Wu, Z. (2017), "Effect of circumferentially nonuniform lateral tension on bond behavior between plain round bars and concrete: Analytical study", *J. Struct. Eng.*, **143**(12), 34-54.
- Ziaei-Nia, A., Shariati, M. and Salehabadi, E. (2018), "Dynamic mix design optimization of high-performance concrete", *Steel Compos. Struct.*, **29**(1), 67-75.  
<https://doi.org/10.12989/scs.2018.29.1.067>.
- Zong-cai, D., Daud, J.R. and Chang-xing, Y. (2014), "Bonding between high strength rebar and reactive powder concrete", *Comput. Concrete*, **13**(3), 411-421.  
<http://dx.doi.org/10.12989/cac.2014.13.3.411>.